第 33 卷第 12 期　　焊　接　学　报　　Vol. 33　No. 12
2012 年 12 月　　TRANSACTIONS OF THE CHINA WELDING INSTITUTION　　December　2012

TGO 界面特征对热障涂层残余应力的影响

韩志勇，　张　华，　王志平
（中国民航大学 天津市民用航空器适航与维修重点实验室，天津　300300）

韩志勇

摘　要：采用非线性有限元方法模拟计算了热障涂层中陶瓷层（TCC）及粘结层（BC）与热生长氧化物（TGO）层界面的残余应力的分布，计算过程中，考虑到了材料物性的非线性特征及界面形貌特征的影响. 结果表明，形貌单元尺寸及分布密度对 TGO 界面应力有明显的影响，TCC/TGO 界面的应力大于 BC/TGO 界面的应力. 在锥形坑形貌中心尖点处存在应力集中现象，且呈现最大应力值，是涂层失效的危险点，并且残余应力值随着界面形貌分布密度的增加而减小.

关键词：热障涂层；非线性计算；界面形貌；热生长氧化物
中图分类号：TG172.6　　**文献标识码**：A　　**文章编号**：0253－360X(2012)12－0033－04

0　序　　言

典型的热障涂层（TBCs）结构由陶瓷层（TCC）、粘结层（BC）和金属基体组成，由于其优越的耐高温、耐腐蚀、耐磨损和低导热等性能，热障涂层广泛应用于热端部件的表面[1－3]. 在实际应用过程中，由于氧化作用，陶瓷层和粘结层之间通常还会生成一层很薄的成分主要为 Al_2O_3 的热生长氧化物（TGO），TGO 的形成可以起到热障涂层抗热腐蚀的作用[4].

如何解决和控制结合界面的开裂剥离是提高热障涂层寿命的主要研究方向. 在高周热循环作用下，TGO 的成分以及形态发生变化，导致 TGO 的界面产生很大的残余压应力，应力增加到一定程度就很容易引起涂层剥落[4,5]，这是热障涂层失效的重要原因，同时也是热障涂层在应用中亟待解决的问题之一.

界面粗糙化有利于增强界面的机械结合力从而提高界面的结合强度，是提高发动机中热障涂层寿命的有效措施. 然而界面粗糙化的同时会改变热障涂层系统中由于热应变失配而导致的残余应力的分布状况，产生了促使陶瓷层内裂纹扩展和最后剥离的应力[5]. 同时由于 TGO 的生长极其复杂，因此热障涂层系统界面形貌以及 TGO 生长与界面残余应力关系的研究具有重要意义. 关于热障涂层系统残余应力的研究与预测问题的试验研究相对复杂，随着计算机技术的发展国内外学者对涂层形貌与残余应力分布关系的模拟技术进行了大量的探索和研究，取得了有相当参考价值的成果[6,7]. 利用 ABAQUS 有限元分析软件，引入了材料的热物性特征，模拟计算了 TGO 生长下陶瓷层、粘结层间锥形形貌单元尺寸和分布密度与热障涂层残余应力的关系，对涂层的失效方式进行初步分析，对涂层制备过程中表面形貌的控制具有指导意义.

1　模型建立

文中的研究对象为高温热循环条件下，等离子喷涂双层热障涂层中热氧化层形貌单元尺寸及分布密度与残余应力分布的关系，涂层界面形貌如图 1 所示[8]. 计算模型中，其陶瓷层（内含质量分数为 8% Y_2O_3 的 ZrO_2）厚度为 250 μm，粘结层（Ni-22Cr-10Al-1Y）厚度为 100 μm，TGO 层的厚度为 1 μm. 粘结层表面近似均匀分布着典型的凹坑形貌. 由于

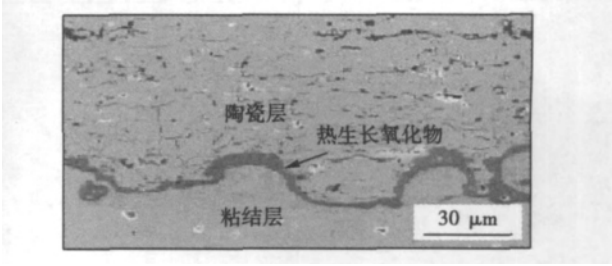

图 1　高温热循环处理后热障涂层界面 SEM 图像
Fig. 1　SEM image of interface after thermal cycling

收稿日期：2011－11－03
基金项目：中央高校基本科研基金资助项目（ZXH2010C009）

基体的厚度尺寸远远大于粘结层和涂层的厚度尺寸，计算模型只取粘结层、TGO 和陶瓷层，涂层截面结构计算模型如图 2. 模型的形貌周期为 d，锥形坑截面圆直径为 $2r$.

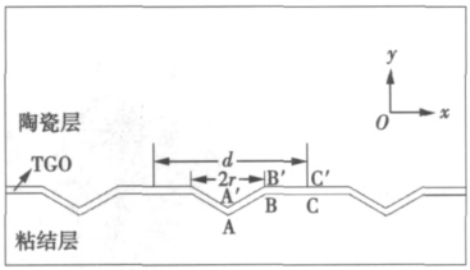

图 2 TGO 均匀生长的涂层截面示意图

Fig. 2 Sketch of coating in uniform growth

模型中首先分析在相同分布密度下的圆锥凹坑单元尖角程度及尺寸对 TCC/TGO 界面及 BC/TGO 界面残余应力的影响. 计算过程中，水平 x-z 平面内 x 方向和 z 方向分别取三个周期单元，计算形貌单元与残余应力的关系. 然后增加形貌单元的分布密度，分析单元分布密度对残余应力与界面粗糙度的关系. 计算过程中，采用三维八节点实体减缩积分单元(C3D8R) .

热障涂层在高温阶段，基体和粘接层金属会发生蠕变，假定在冷却之前涂层处于应力自由状态. 由于涂层厚度相对较小，可以近似认为系统在高温无应力状态时为均匀的温度场，冷却时温度均匀下降至室温 25 ℃，在整个计算过程中涂层周围空间中的温度分布是均衡的. 考虑到对称性，模型的 x-y 面和 y-z 面实行对称约束. 由于计算中没有考虑基体，模型粘结层底部设置为完全固定. 此外建立有限元模型时，为了简化计算并且不失研究问题的代表性，作了如下假设: 整个涂层系统没有缺陷; 陶瓷层和结合层在界面处为完全粘结; 在降温过程中，涂层系统不产生塑性变形和蠕变，所有的材料属性都是完全弹性的; 每层材料内各向同性; 重点考虑了温度变化引起的涂层物性参数的变化，其物性参数如表 1 所示[9,10] .

表 1 陶瓷层、热生长氧化物及粘结层的热力学参数

Table 1 Thermodynamic parameters of TCC, TGO and BC

材料	温度 T/℃	弹性模量 E/GPa	泊松比 μ	线膨胀系数 α_l/ 10^{-5} K^{-1}	热导率 λ/($W \cdot m^{-1} \cdot K^{-1}$)	密度 ρ/($kg \cdot m^{-3}$)	比热容 c/($J \cdot kg^{-1} \cdot K^{-1}$)
TCC	20	48	0.1	0.9	1.2	5 000	450
	200	47	0.1	0.92	1.19	—	—
	400	44	0.1	0.96	1.18	—	—
	600	40	0.11	1.01	1.15	—	—
	800	34	0.11	1.08	1.16	—	—
	1 000	26	0.12	1.17	1.14	4 840	—
TGO	0	387.8	0.257	0.592	—	3 800	830
	22	386	0.257	0.6	36	—	—
	566	347.6	0.257	0.8	9.9	—	—
	1 149	312.1	0.257	0.89	5.89	—	—
BC	20	200	0.3	1.36	5.8	7 800	400
	200	190	0.3	1.42	7.5	—	—
	400	175	0.31	1.46	9.5	—	—
	600	160	0.31	1.52	12	—	—
	800	145	0.32	1.61	14.5	—	—
	1 000	120	0.33	1.72	16.2	7 430	—

2 计算结果与分析讨论

2.1 形貌单元尺寸与界面应力的关系

一般认为，垂直于界面的残余拉应力 σ_{22} 容易导致陶瓷层剥落[11] . 对于图 2 所示的界面形貌，取粘结层表面凹坑形貌截面圆半径 r 为 50 μm，深度 h 为 30 μm，形貌周期 d 为 200 μm. 残余应力 σ_{22} 的分布云图如图 3 所示. 由于应力分布的对称性，在半个周期内，图 2 所示计算路径 A→B→C 及 A′→B′→C′上均匀取 20 个点，TGO 与粘结层和陶瓷层界面的残余应力如图 4 所示. 其中 A 和 A′为第 1 结点，B 和 B′为第 12 结点，C 和 C′为第 20 结点. 图 3 和图 4 显示，A 和 A′处存在应力集中，应力最大值分别达

到 832 MPa 和 695 MPa. 随着计算路径远离中心点，拉应力显著降低，TGO/BC 界面的应力降低速度远远大于 TGO/TCC 界面应力的变化. 在角点 B 和 B′ 附近变为压应力，在 B，C 段应力变化不明显，并且 TGO/TCC 界面的应力要大于 TGO/BC 界面的残余应力. 由此可以看出，在 TGO 界面 A 处是涂层失效的危险点.

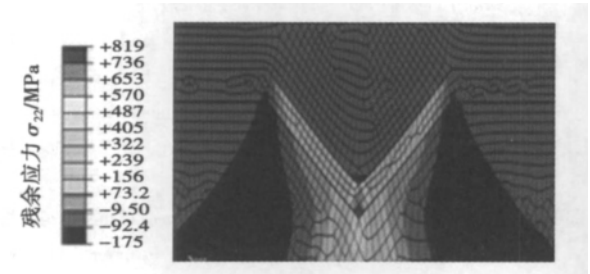

图 3　残余应力云图

Fig. 3　Contour plot of residual stress σ_{22}

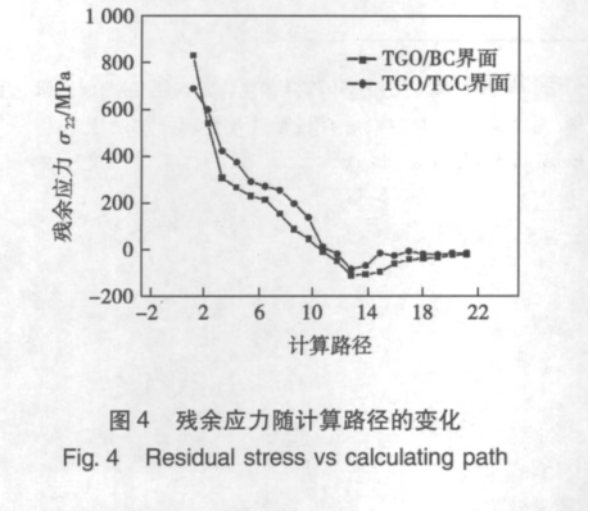

图 4　残余应力随计算路径的变化

Fig. 4　Residual stress vs calculating path

2.2　形貌单元尺寸变化与界面 A 点应力的关系

为了研究形貌尺寸大小与残余应力 σ_{22} 的关系，计算了危险点 A 处残余应力随形貌深度 h 和半径 r 以及它们比值之间的变化关系. 其中坑深 h 由 10 μm 变至 50 μm，随着形貌深度的增加，h/r 的比值由 0.1 变至 1 计算结果如图 5a 所示. 可以看出，在截面圆半径一定的情况下，应力随着形貌深度 h 的增加基本线性增加. 对于较大尺寸的形貌，随着深度的增加，变化更为显著，当半径为 50 μm，h/r 比值达到 1 时，应力达到最大值 1 263 MPa. 而在 h/r 比值一定的情况下，σ_{22} 随着 h 和 r 的增加而增大. 说明界面形貌尺寸增加在增大涂层结合力的同时，残余应力会同时增大.

2.3　形貌分布密度与界面 A 点应力的关系

形貌单元数量的增加有利于界面结合力的增大，但是形貌数量增加易导致引起涂层失效的凸起形貌端点的出现. 为此研究了形貌分布密度与残余应力的关系. 对于图 2 所示的凹形形貌单元，粘结层单位表面凹坑形貌数量增加到五个形貌单元，截面圆半径 r 同样由 10 μm 变至 50 μm，h/r 由 0.1 变至 1，形貌中心 A 处的应力随形貌尺寸的变化如图 5b 所示. 由图 5a 与图 5b 可以看出，随着界面形貌数目的增加，单个形貌单元中心 A 点残余应力的变化趋势基本一致，残余应力随着形貌密度的增加而减小.

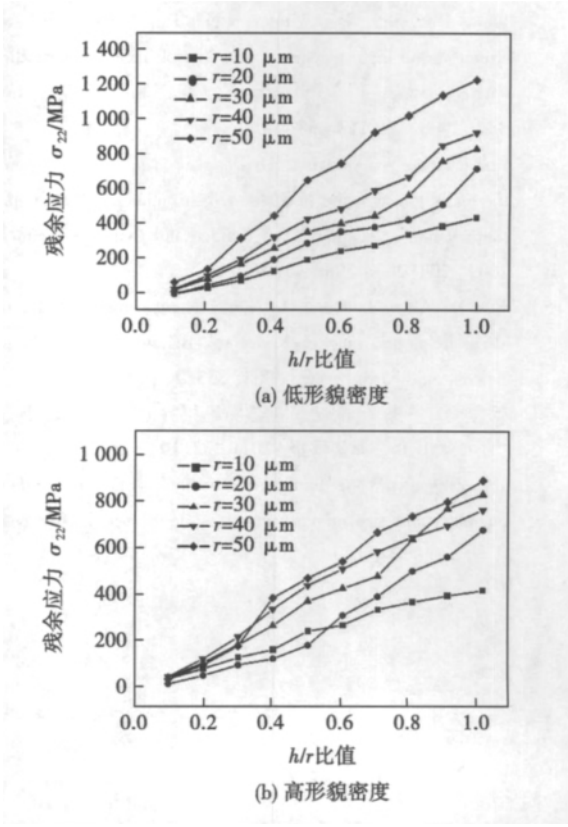

图 5　残余应力随形貌尺寸的变化

Fig. 5　σ_{22} vs dimension of topograph

3　结　　论

(1) 高温热循环后，热生长氧化物 TGO/BC 界面和 TGO/TCC 界面存在较大的残余应力，TGO 与陶瓷层界面处应力大于 TGO 与粘结层界面的残余应力，TGO/BC 界面形貌中心处存在应力集中，是涂层失效的危险点.

(2) 界面形貌单元尺寸对界面应力有明显的影响，残余应力随着形貌绝对深度的增加而增大. 在截面半径与形貌深度比值一定的情况下，残余应力随着绝对尺寸的增加而增大.

(3) 界面形貌单元分布密度对界面应力有一定的影响，涂层失效危险点的残余应力随着形貌密度的增加而减小.

参考文献:

[1] Ma W, Jarligo M O, Mack D E, *et al*. New generation perovskite thermal barrier coating materials [J]. Journal of Thermal Spray Technology, 2008, 17(5-6): 831-837.

[2] Stover D, Funke C. Directions of the development of thermal barrier coatings in energy applications [J]. Journal of Materials Processing Technology, 1999, 92-93(30): 195-202.

[3] **王红英, 郝云飞, 陈 辉. 纳米氧化锆热障涂层组织结构和高温稳定性能分析** [J]. **焊接学报**, 2008, 29(11): 37-40.
Wang Hongying, Hao Yunfei, Chen Hui. Analysis on microstructure and high temperature stability of nanostructured thermal barrier coatings [J]. Transactions of the China Welding Institution, 2008, 29(11): 37-40.

[4] Che Chang, Wu Guoqing, Qi Hongyu, *et al*. Uneven growth of thermally grown oxide and stress distribution in plasma-sprayed thermal barrier coatings [J]. Surface and Coatings Technology, 2009, 203(20): 3088-3091.

[5] Sfar K, Aktaa J, Munz D. Numerical investigations of residual stress fields and crack behavior in TBC systems [J]. Materials Science and Engineering, 2002, 333(2): 351-360.

[6] **韩志勇, 王志平, 陈亚军. 热障涂层界面形貌和尺寸对热应力的影响** [J]. **焊接学报**, 2011, 32(10): 21-24.
Han Zhiyong, Wang Zhiping, Chen Yajun. Effect of interface topography and size on thermal stress in thermal barrier coatings [J]. Transactions of the China Welding Institution, 2011, 32(10): 21-24.

[7] **侯平均, 王汉功, 汪刘应. 等离子喷涂双层热障涂层沉积过程的数值模拟** [J]. **焊接学报**, 2009, 30(11): 97-100.
Hou Pingjun, Wang Hangong, Wang Liuying. Numerical simulation on deposition process of duplex thermal barrier coating by plasma spraying [J]. Transactions of the China Welding Institution, 2009, 30(11): 97-100.

[8] Hsueh C H, Edwin R, Fuller Jr. Residual stresses in thermal barrier coatings: effects of interface asperity curvature/height and oxide thickness [J]. Materials Science and Engineering A, 2000, 283(1-2): 46-55.

[9] Karlsson A M, Levi C G, Evans A G. A model study of displacement instabilities during cyclic oxidation [J]. Acta Materialia, 2002, 50(6): 1263-1273.

[10] Karlsson A M, Xu T, Evans A G. The effect of the thermal barrier coating on the displacement instability in thermal barrier systems [J]. Acta Materialia, 2002, 50(5): 1211-1218.

[11] McCarthy C T, McCarthy M A, Lawlor V P. Progressive damage analysis of multi-bolt composite joints with variable bolt-hole clearances [J]. Composites Part B: Engineering, 2005, 36(4): 290-305.

作者简介: **韩志勇,男,**1970 **年出生,博士,副教授,硕士研究生导师. 主要研究方向为涂层材料制备与计算. 发表论文** 10 **余篇.**
Email: zyhan@cauc.edu.cn

Abstract: TCS345, T4003, Nirosta 4003 and JFE410RW ferritic stainless steels were welded by ER-309 welding wire in this paper. The microstructure of their base metal and joint were analyzed by metallographic approach, and the corrosion resistance of base metal and joints was evaluated by electrochemical corrosion tests. The experimental results demonstrated that, compared with that of Nirosta 4003 and JFE410RW, low content of Ti and Mn elements were found in TCS345 and T4003 ferritic stainless steels, especially the low content of Ti, which resulted in the obvious grain growth of TCS345 and T4003 ferritic stainless steels. Moreover, the welding joints of ferritic stainless steels exhibited big heat affected zone (HAZ). Compared with the microstructure of base metal, the HAZ area showed obvious large grains. As far as TCS345 is concerned, obvious grain growth is observed. In the case of Nirosta 4003 and JFE410RW, they exhibited smaller size of grain than TCS345. In 1mol/L Na_2SO_4 solution, the corrosion resistance of TCS345 and JFE410RW is better than that of T4003 and Nirosta 4003.

Key words: ferritic stainless steel; welding joint; metallographic microstructure; corrosion resistance

Effect of microplasma spraying working gas on crystallinity of HA coatings ZHAO Qiuying[1], HE Dingyong[2], LIU Yan[2], LI Xiaoyan[2], CHEN Shujun[3] (1. Postdoctoral Research Station of Mechanical Engineering, Beijing University of Technology, Beijing 100124, China; 2. College of Materials Science and Engineering, Beijing University of Technology, Beijing 100124, China; 3. College of Mechanical Engineering and Applied Electronics Technology, Beijing University of Technology, Beijing 100124, China). pp 23 - 27

Abstract: Hydroxyapatite (HA) coatings were prepared on Ti-6Al-4V substrate by using the method of microplasma spraying. Commercially pure argon gas and helium/argon (50% in volume) mixed gas were used as working gas in the spraying processing respectively. The surface morphology, phase compositions and degree of crystallinity of the coatings were examined by scanning electron microscope (SEM) and X-ray diffraction (XRD). Results show that less impurity phases and no TTCP and CaO phases were found in the coatings. The crystallinity of coatings is higher than 70%, which is beneficial for implantation materials stability in vitro and vivo. The enthalpy of microplasma arc in which helium/argon mixed is used as working gas is higher than that in which commercially pure argon gas is used. The crystalline phases in the former coatings mainly consist of recrystallization grains while the latter coatings were mainly made up of lots of unmelted HA particles.

Key words: microplasma spraying; hydroxyapatite coatings; helium/argon mixed gas; crystallinity

Development of hybrid laser + double wire MIG/MAG welding system and process ZHU Yanli[1], LI Huan[1], YANG Lijun[1], GAO Ying[2] (1. Tianjin Key Laboratory of Advanced Joining Technology, Tianjin University, Tianjin 300072, China; 2. Tianjin Key Laboratory of High Speed Cutting and Precision Machining, Tianjin University of Technology and Education, Tianjin 300222, China). pp 28 - 32

Abstract: In order to study the process of laser + double wire welding, the hybrid laser + double wire MIG/MAG welding system was constructed. The method of pulsed controlling of the powers which are mutually independent is alternative. The welding experiments were also carried out with this system in this paper. The double current signals, voltage signals and high-speed camera signals were synchronously collected. The result shows that the hybrid laser + double wire MIG/MAG welding system can carry out stable welding and the appearance of the weld is good. The diversifications of voltage signals were obvious and the stability of voltage signals was improved as a result of injection of the laser power.

Key words: hybrid laser + double wire MIG/MAG welding; electric signals; high-speed camera

Effect of TGO topography on TBCs residual stresses HAN Zhiyong, ZHANG Hua, WANG Zhiping (Tianjin Key Laboratory for Civil Aircraft Airworthiness and Maintenance, Civil Aviation University of China, Tianjin 300300, China). pp 33 - 36

Abstract: By using nonlinear finite element model, the residual stress distribution which was affected by interface topography of top ceramic coat (TCC), bond coat (BC) and thermally-growth oxide (TGO) interface area in thermal barrier coatings (TBCs) system was calculated. In the process of calculation, thermodynamic parameters of TCC, TGO and BC were considered. The calculating results show that the residual stress of TGO interface is affected by interface topography unit size and topography distribution density obviously. The stress on TCC/TGO interface is greater than that on BC/TGO interface. Stress concentrates at the tip of cone topography center and reaches the maximum value, which becomes the dangerous point for failure of thermal barrier coatings system. The residual stress level decreases with the increasing of topography quantity.

Key words: thermal barrier coatings; nonlinear calculation; interface topography; TGO

Study on performance of 6156 skin butt joint with laser beam welding ZHAN Xiaohong[1,2], CHEN Jie[1], TAO Wang[3], YANG Zhibin[3], WEI Yanhong[2,3], CHEN Yanbin[3], OU Wenmin[2] (1. Shanghai Aircraft Manufacturing Co., Ltd, Shanghai 200436, China; 2. College of Material Science and Technology, Nanjing University of Aeronautics and Astronautics, Nanjing 210016, China; 3. State Key Laboratory of Advanced Welding Production Technology, Harbin Institute of Technology, Harbin 150001, China). pp 37 - 40

Abstract: The laser beam welding characteristics of 6156 aluminum butt joint with and without filling wire are investigated. The factors which influence the weld appearance and weld width are analyzed. The variety rule of tensile and fatigue strength are discussed. The results show that the appearance of the weld joint with filler metal is better than the one without filler metal. The maximum weld gap tolerance of the weld joint with filler metal increases to 0.7 mm. The strength of weld joint without heat treatment is 314.3 MPa which is 81.3% of base metal. Laser welding of aluminum is a favorable weld technology with the characteristics of high speed, fine weld appearance and wide weldability.

Key words: laser beam welding; aluminum alloy; butt